

Torque Modeling of a Spherical Actuator Based on Lorentz Force Law

Liang Yan, I-Ming Chen and Chee Kian Lim
School of Mechanical and
Production Engineering
Nanyang Technological University
Singapore 639798
pg00350830@ntu.edu.sg

Guilin Yang, Wei Lin
Mechatronics Group
Singapore Institute of
Manufacturing Technology
Singapore 638075
glyang@SIMTech.a-star.edu.sg

Kok-Meng Lee
George W. Woodruff School of
Mechanical Engineering
Georgia Institute of Technology
Atlanta, Georgia, USA 30332-0405
kokmeng.lee@me.gatech.edu

Abstract—An actuator with 3-DOF spherical motion is developed based on layered arrangement of stator coils and rotor poles. Due to the use of air-core coils and permanent magnet poles, the torque model of the actuator cannot be obtained by traditional coenergy approach. This paper describes a generic torque modeling method based on Lorentz force law. The closed-form solution of the torque model is derived from the scalar potentials of the magnetic field. Experimental study on the torque model is carried out. A comparison between the closed-form solution and the experimental result shows that the proposed torque model is valid and can be used for real-time control.

I. INTRODUCTION

The concept of the spherical actuator has been proposed by several researchers to achieve a smooth 3-DOF rotational motion in only one joint. A spherical motor manipulated by four wires is developed by Nagasawa *et al* [1]. Essentially this 3-DOF motion is realized by four single-axis motors connected with the rotor. Multi-degree of freedom spherical ultrasonic motor is a fascinating topic proposed by Toyama *et al* [2]. The primary disadvantage of the ultrasonic motor is the instability of the motor due to the wear of frictional material utilized in operation. Chirikjian *et al.* developed a spherical stepper motor [3]. This stepper motor possesses a rotor as big as 12 inches diameter and its torque is not desirable. Lee *et al.* have developed a variable-reluctance spherical motor [4], which has a compact size. However, a nonlinear torque model relates the current inputs and the torque output, which is not favored by real-time control [5]. It is worth mentioning that spherical permanent magnet actuators which can achieve either 2-DOF motion or 3-DOF motion are developed by Wang *et al* [6][7]. However, in these actuators, only some simple cases such as two or four permanent-magnet (PM) poles and three or four windings have been considered. In addition the rotor surface is basically regarded as completely consisting of magnetized rare earth materials (NdFeB) that has a high density (7.5g/mm^3). This increases both the moment of inertia of the rotor and the cost of system.

This paper presents a spherical actuator with generalized structure that consists of a ball-shaped rotor with a full circle of PM poles and a spherical shell like stator with two layers of circumferential air-core coils. The PMs of

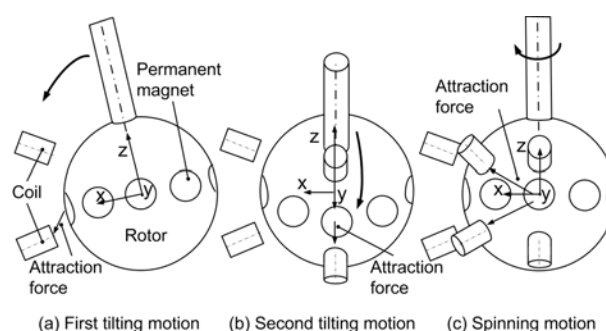


Fig. 1. 3-DOF motion of the spherical actuator

rare earth materials can generate high flux density within the actuator, and the air-core coils may simplify the torque model of the spherical actuator. The basic working principle of the actuator is shown in Fig. 1. Activating a pair of coils in two longitudinal directions, the rotor creates tilting motion in two orthogonal directions as shown in Fig. 1(a) and (b). Activating the rest of the circumferential coils, the rotor can spin about its own axis. Therefore, by varying the input currents of the coils, the rotor can produce any desirable spherical motion in three dimensional space. By using this configuration, it is possible to incorporate more layers of coils and PMs into the stator and the rotor to achieve higher resolution and larger working range.

To develop a servo system for the position and speed control of the spherical actuator, the torque model of the actuator is necessary. Most of the electromagnetic actuators possess a closed magnetic flux loop between the rotor and the stator and most of the magnetic energy is stored inside the narrow airgap among the poles [4]. Therefore, it is possible to use coenergy approach [8] to formulate the torque model of the actuator. The torque model can be obtained by differentiating the magnetic energy equation with respect to the angular displacement of the rotor. However, because of the use of air-core coils in this PM spherical actuator, the energy stored in the airgap cannot be formulated easily. Therefore, the coenergy method becomes ineffective. Wang *et al.* proposed a torque modeling method based on Lorentz force law [7][9] in a PM spherical actuator. However, only simple patterns of the rotor and stator poles have been considered. In this article, we propose an generic torque model based on Lorentz

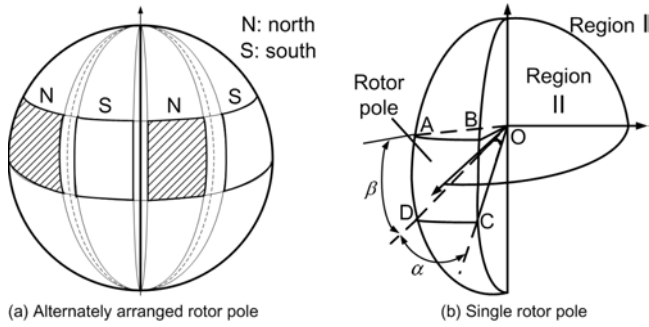


Fig. 2. Arrangement of the rotor poles

force law. This method has advantages as follows. (1) The PM pole is specified by several parameters so that the size can be varied and optimized. This also indicates that the rotor surface is not necessary covered by rare earth material entirely. (2) Cutting off unnecessary materials in PM poles decreases the moment of inertia of the rotor which is favored by system dynamics. (3) In our study, we find out that by selecting appropriate parameters of the PM poles, the dihedral shaped PM poles that are used in modeling can be replaced by cylindrical shaped PMs. This replacement can simplify the fabrication and reduce the cost markedly. (4) This design concept and corresponding modeling method allow more layers of PM poles to be built into the rotor to achieve high torque as well as high precision motion. (5) A closed-form solution of the torque model of the actuator can be obtained, which is favored by real-time control.

II. FORMULATION OF MAGNETIC FIELD

Our previous study [10] shows that the magnetic field of the PM pole (5kG) is dominant compare with the flux density caused by the air-core coil (50G for 2A current). Hence, the focus is on the magnetic field produced by the rotor poles.

A. Arrangement of Rotor Poles

The PM poles in alternate magnetization direction are placed around the equator of the rotor as shown in Fig. 2(a). This arrangement leads to the periodical variation of the magnetic field distribution circumvent the rotor. One difficulty encountered in this configuration is how to deal with the rest regions in the rotor other than the rotor poles because those areas regions are made of aluminum, not of rare earth material. Since the permeability of the rare earth material, aluminium, and air are all about the same, we can assume the remaining areas are made up of rare earth material without magnetization. In other words, the rotor can be treated as a ball made of completely rare earth material with only PM poles along the equator. Based on this, the integration operation can be performed within the entire rotor volume.

Figure 2(b) presents the shape of a single rotor pole, i.e. the approximate dihedral cone $OABCD$. The dihedral cone is defined by two parameters: α and β . This type of

the rotor pole structure has several advantages. (1) The volume of the rotor pole is now described in spherical coordinates, which facilitates the computation of the torque. (2) By changing the parameters of the dihedral cone α and β , we can model the rotor poles with different dimensions. This will facilitate the study of optimal magnet-pole pattern. (3) Customarily design the shape of the PM poles to obtain special pole geometry becomes possible. For example, let $\beta = 180^\circ$, we can have a sector magnet.

B. Scalar Potential

Denote the outer and inner regions of the rotor as Region I and Region II respectively as shown in Fig. 2(b). On account of the material properties, we have following equations for these two regions respectively [7]:

$$\mathbf{B}_I = \mu_0 \mathbf{H}_I, \quad (1)$$

$$\mathbf{B}_{II} = \mu_m \mathbf{H}_{II} + \mu_0 \mathbf{M}_0, \quad (2)$$

where \mathbf{H} and \mathbf{B} represent the magnetic field intensity (A/m) and the flux density (T) respectively, $\mathbf{M}_0 = \mathbf{B}_{rem}/\mu_0$ is the residual magnetization vector (A/m), \mathbf{B}_{rem} is the remanence (T), μ_0 is the permeability of free space which has the value of $4\pi \times 10^{-7}$ H/m, $\mu_m = \mu_r \mu_0$ is the recoil permeability of the permanent magnet, the dimensionless quantity μ_r is the relative recoil permeability. Note that Eqn. (2) indicates a linear demagnetization characteristic of the PM in the BH curve and μ_r is a constant. This equation is applicable to the magnetized portion within Region II .

As magnetic field is solenoidal, according to Maxwell equations, we obtain the following condition outside the rotor in the form of the Laplace equation:

$$\nabla^2 \Phi_I = 0, \quad (3)$$

where Φ is a scalar potential. Similarly, within Region II , the following equation in the form of Poisson's equation can be established:

$$\nabla^2 \Phi_{II} = \nabla \cdot \mathbf{M}_0 / \mu_r. \quad (4)$$

Due to the symmetry of the rotor pole arrangement, the divergence of the residual magnetization vector is equal to zero. Thus the Poisson's equation is equivalent to a Laplace's equation, that is, $\nabla^2 \Phi_{II} = 0$. This relationship indicates that the non-magnetized area within the rotor has no effect on the solution of scalar potential. By expanding partial differential equations (3) and (4) in the spherical coordinates (r, θ, ϕ) illustrated in Fig. 3, we can obtain the solutions of the scalar potentials as following [11]

$$\Phi_i = \sum_{n=0}^{\infty} \sum_{m=-n}^n (\kappa_{ni}^m r^n + \xi_{ni}^m r^{-(n+1)}) Y_n^m(\theta, \phi), \quad (5)$$

where $i = I, II$; κ_{ni}^m and ξ_{ni}^m are constants related to boundary conditions. And Y_n^m , the solutions of the angular portion of the Laplace's equation, are the spherical harmonic functions defined by

$$Y_n^m(\theta, \phi) = \sqrt{\frac{2n+1}{4\pi} \frac{(n-m)!}{(n+m)!}} P_n^m(\cos \theta) e^{im\phi},$$

where $P_n^m(\cos \theta)$ are associated Legendre functions [12], n and m are integers with $-n \leq m \leq n$. Note that spherical harmonics are complex valued functions.

C. Spherical Harmonic Expansion of M_{0r}

The radial component of the residual magnetization vector, $M_{0r}(\theta, \phi)$, can be expressed as an expansion of spherical harmonic functions $Y_n^m(\theta, \phi)$ as follows:

$$M_{0r}^s(\theta, \phi) = \sum_{n=0}^{\infty} \sum_{m=-n}^n C_{nm} Y_n^m(\theta, \phi), \quad (6)$$

where C_{nm} are coefficients determined from the surface integral of the following form:

$$C_{nm} = \int_0^{\pi} \int_0^{2\pi} M_{0r}(\theta, \phi) Y_n^{m*}(\theta, \phi) \sin \theta d\theta d\phi, \quad (7)$$

where the asterisk of $Y_n^{m*}(\theta, \phi)$ denotes the complex conjugate. Figure 4 illustrates the equatorial plane of the rotor in Cartesian coordinates as well as spherical coordinates. Let M_0 be the magnitude of \mathbf{M}_0 . The constituent of the residual magnetization vector in the radial direction r is

$$M_{0r} = (-1)^{p-1} M_0 \cos\left(\phi - \frac{\alpha}{2} - \frac{\pi}{4}(p-1)\right) \sin \theta, \quad p=1, 2, \dots, 8. \quad (8)$$

Note that Eqn. (8) is only valid within the rotor poles. Hence, the residual magnetization vector is confined in

$$\frac{\pi}{4}(p-1) < \phi < \frac{\pi}{4}(p-1) + \alpha, \quad \frac{\pi}{2} - \frac{\beta}{2} < \theta < \frac{\pi}{2} + \frac{\beta}{2}.$$

For the rest non-magnetized regions on the rotor, M_{0r} is equal to zero. Substituting Eqn. (8) into Eqn. (7) gives

$$C_{nm} = M_0 \int_0^{2\pi} f(\phi) e^{im\phi} d\phi \int_0^{\pi} \sqrt{\frac{2n+1}{4\pi} \frac{(n-m)!}{(n+m)!}} P_n^m(\cos \theta) \sin^2 \theta d\theta \quad (9)$$

where $f(\phi) = (-1)^{(p-1)} \cos\left(\phi - \frac{\alpha}{2} - \frac{\pi}{4}(p-1)\right)$, $p = 1, 2, \dots, 8$. Through computation, we observe that $C_{nm} \neq 0$ if and only if $m = \pm 4, \pm 12, \pm 20, \dots$. Thus the fundamental terms are at $n = 4$ and $m = \pm 4$. To simplify the calculation, only the fundamental terms are used for the derivation of the magnetic field. Denote the integral of $\int_0^{2\pi} f(\phi) e^{im\phi} d\phi$ in Eqn. (9) at $m = 4$ and $m = -4$ as $a + bi$ and $a - bi$ respectively. The integral of $\int_0^{\pi} \sqrt{\frac{2n+1}{4\pi} \frac{(n-m)!}{(n+m)!}} \sin \theta P_n^m(\cos \theta) \sin \theta d\theta$ in Eqn. (9) is a

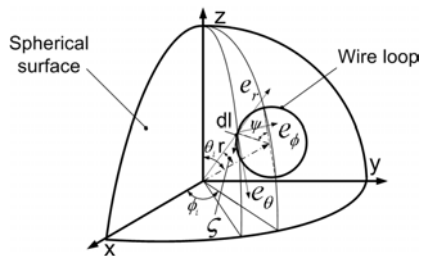


Fig. 3. Spherical coordinates defined on the rotor

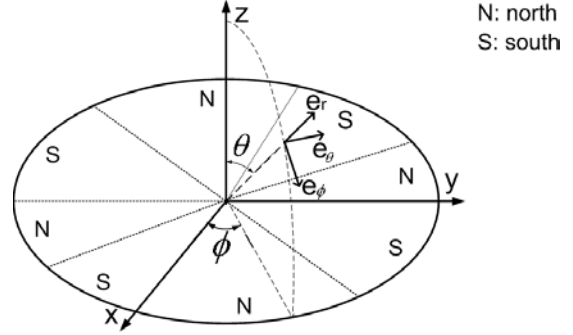


Fig. 4. Rotor poles in spherical coordinates on equatorial plane

real number having the form of $c/\sqrt{\pi}$. Combining the two integrals together gives:

$$C_{4,4} = M_0 \frac{1}{\sqrt{\pi}} (a + bi)c, \quad C_{4,-4} = M_0 \frac{1}{\sqrt{\pi}} (a - bi)c, \quad (10)$$

where $c_{4,-4}$ is the conjugated value of $c_{4,4}$. Therefore,

$$M_{0r}^s(\theta, \phi) = c_{4,-4} Y_4^{-4}(\theta, \phi) + c_{4,4} Y_4^4(\theta, \phi),$$

where

$$Y_4^{-4} = \frac{3}{16} \sqrt{\frac{35}{2\pi}} \sin^4 \theta e^{-4i\phi}, \quad Y_4^4 = \frac{3}{16} \sqrt{\frac{35}{2\pi}} \sin^4 \theta e^{4i\phi}.$$

D. Boundary Conditions

Here we study the constants in scalar potentials related to the boundary conditions (BC) in Eqn. (5): κ_{nI}^m , κ_{nII}^m , ξ_{nI}^m and ξ_{nII}^m . Considering Region I and Region II of the rotor, there are five boundary conditions,

$$\begin{aligned} \text{BC-1} : \Phi_I|_{r \rightarrow \infty} &= 0, & \text{BC-2} : \Phi_{II}|_{r=0} &\neq \infty, \\ \text{BC-3} : H_{\theta I} &= H_{\theta II}|_{r=R_r}, & \text{BC-4} : H_{\phi I} &= H_{\phi II}|_{r=R_r}, \\ \text{BC-5} : B_{rI} &= B_{rII}|_{r=R_r}, \end{aligned}$$

where R_r is the radius of the rotor. BC-1 means that $\kappa_{nI}^m = 0$ in Eqn. (5). Similarly, BC-2 indicates that $\xi_{nII}^m = 0$. Components of magnetic field intensity can be computed in the following manner:

$$H_r = -\frac{\partial \Phi}{\partial r}, \quad H_\theta = -\frac{1}{r} \frac{\partial \Phi}{\partial \theta}, \quad H_\phi = -\frac{1}{r \sin \theta} \frac{\partial \Phi}{\partial \phi}. \quad (11)$$

Now we consider the remaining BCs. BC-3 results in

$$\kappa_{nII}^m R_r^{2n+1} = \xi_{nI}^m. \quad (12)$$

Similarly, BC-4 gives the same result as Eqn. (12). BC-5 can be written specifically as

$$-\mu_r \frac{\partial \Phi_{II}}{\partial r} \Big|_{r=R_r} + M_{0r} = -\frac{\partial \Phi_I}{\partial r} \Big|_{r=R_r}, \quad (13)$$

The first term on the left-hand side and the term on the right-hand side of Eqn. (13) are both compositions of spherical harmonics. Thus, forming M_{0r} in terms of spherical harmonics as shown in the previous section provides the solution to Eqn. (13). Because spherical harmonics are

orthonormal functions [12], Eqn. (13) holds for every pair of n and m . Finally, we have

$$\kappa_{n,II}^m = \frac{C_{nm}}{(n+1+\mu_r n)R_r^{n-1}}, \quad \xi_{nI}^m = \frac{C_{nm}R_r^{n+2}}{(n+1+\mu_r n)}. \quad (14)$$

Particularly, for $n = 4$ and $m = \pm 4$, by substituting Eqn. (10) into Eqn. (14), we obtain

$$\xi_{4I}^4 = \frac{M_0(a+bi)cR_r^6}{\sqrt{\pi}(5+4\mu_r)}, \quad \xi_{4I}^{-4} = \frac{M_0(a-bi)cR_r^6}{\sqrt{\pi}(5+4\mu_r)}. \quad (15)$$

E. Solutions of Scalar Potential and Flux Density

As coils are outside of the rotor, the derivation of the flux density is performed in Region I. Substituting Eqn. (15) into Eqn. (5) and omitting the higher order harmonics yields

$$\Phi_I = M_0 \frac{3}{8\pi} \sqrt{\frac{35}{2}} \frac{cR_r^6}{(5+4\mu_r)} r^{-5} \sin^4 \theta (a \cos 4\phi - b \sin 4\phi). \quad (16)$$

Using Eqn. (11), we obtain the flux density in Region I as

$$B_{rI} = M_0 \frac{15}{8\pi} \sqrt{\frac{35}{2}} \frac{cR_r^6}{(5+4\mu_r)} r^{-6} \sin^4 \theta (a \cos 4\phi - b \sin 4\phi). \quad (17)$$

With reference to Fig. 5, we can determine the direction of the force generated by each component of the flux density. $d\mathbf{l}$ represents the differential length of wire that is tangential to the sphere surface at point O . Only the radial component of the flux density B_{rI} can produce a torque to change the rotor orientation. We focus on B_{rI} in following discussion.

III. TORQUE FORMULATION

Lorentz force law states that the force $d\mathbf{F}$ exerted on differential length $d\mathbf{l}$ of current carrying conductor by external magnetic field \mathbf{B} is equal to the multiplication of the current I and the cross product of $d\mathbf{l}$ and \mathbf{B} , that is, $d\mathbf{F} = I d\mathbf{l} \times \mathbf{B}$. By using Lorentz force law, a torque model relating current inputs of all coils and the magnetic field generated by the rotor is derived in this section. We start with the torque generated by a single coil. To facilitate the integration of torque in spherical coordinates, replace the shape of the coil originally represented by $ABCD$ in Fig. 6 with the conical-shaped coil represented by $A'B'C'D'A'$. It turns out that the volume swept by $ABCD$ is about 97% of that swept by $A'B'C'D'A'$. When considering the wiring on the coils, the total lengths

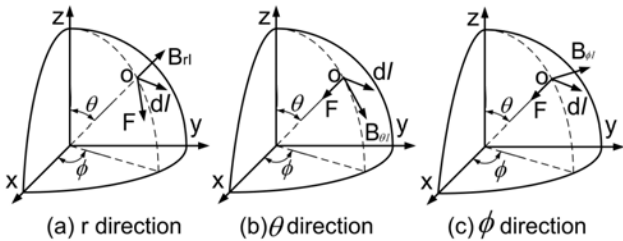


Fig. 5. Force activated by three components of the flux density

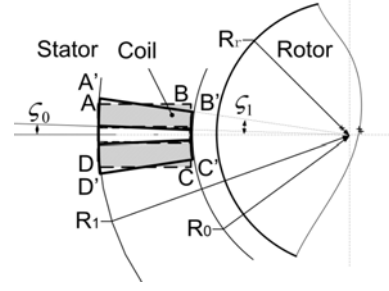


Fig. 6. Approximation of the coil shape (sectional view)

of the wires wrapped around the two coil geometries are about the same. The computation of the torque can be simplified due to the spherical geometry with negligible differences. The torque produced by the i^{th} coil can be calculated as

$$\mathbf{T}_i = -J \int_{R_0}^{R_1} \int_{\zeta_0}^{\zeta_1} \left\{ \int_C r \mathbf{e}_r \times [B_{rI}(r, \theta, \phi) \mathbf{e}_r \times d\mathbf{l}] \right\} r dr d\zeta, \quad (18)$$

where R_0 , R_1 , ζ_0 and ζ_1 are shown in Fig. 6, which are used to specify the volume of the coil; J is current density. The circle on the sphere in Fig. 3 represents one loop of wires on the coil. We know that

$$d\mathbf{l} = r \sin \zeta d\psi (\cos \psi \mathbf{e}_\phi - \sin \psi \mathbf{e}_\theta). \quad (19)$$

Substituting Eqn. (17) and Eqn. (19) into Eqn. (18) results in

$$\mathbf{T}_i = M_0 \frac{15}{8\pi} \sqrt{\frac{35}{2}} \frac{cR_r^6}{(5+4\mu_r)} J \int_{r_0}^{r_1} \int_{\zeta_0}^{\zeta_1} \int_{\zeta=0}^{\zeta=2\pi} r^{-3} \sin^4 \theta (a \cos 4\phi - b \sin 4\phi) \sin \zeta (\cos \psi \mathbf{e}_\phi - \sin \psi \mathbf{e}_\theta) d\psi dr d\zeta, \quad (20)$$

Note that $\sin^4 \theta (a \cos 4\phi - b \sin 4\phi) (\cos \psi \mathbf{e}_\phi - \sin \psi \mathbf{e}_\theta)$ can be written as two terms: $-b \sin^4 \theta \sin 4\phi (\cos \psi \mathbf{e}_\phi - \sin \psi \mathbf{e}_\theta)$ and $a \sin^4 \theta \cos 4\phi (\cos \psi \mathbf{e}_\phi - \sin \psi \mathbf{e}_\theta)$. Denote them as $D_1(\theta, \phi)$ and $D_2(\theta, \phi)$ respectively. Let θ_i and ϕ_i be the orientation of the i^{th} coil with respect to the spherical coordinates defined on the rotor as shown in Fig. 3. We can express the Cartesian coordinates of the differential element on i^{th} coil, x , y and z , in terms of ζ , ψ , θ_i and ϕ_i .

$$\begin{aligned} x &= r \cos \zeta \sin \theta_i \cos \phi_i - r \sin \zeta \cos \psi \cos \theta_i \cos \phi_i + r \sin \zeta \sin \psi \sin \phi_i, \\ y &= r \cos \zeta \sin \theta_i \sin \phi_i - r \sin \zeta \cos \psi \cos \theta_i \sin \phi_i - r \sin \zeta \sin \psi \cos \phi_i, \\ z &= r \cos \zeta \cos \theta_i + r \sin \zeta \cos \psi \sin \theta_i. \end{aligned} \quad (21)$$

Recall the relationship of the Cartesian coordinates, x , y , z and spherical coordinates θ and ϕ ,

$$\cos \phi = \frac{x}{r \sin \theta}, \quad \sin \phi = \frac{y}{r \sin \theta}. \quad (22)$$

Substituting Eqn. (22) into $D_1(\theta, \phi)$ gives

$$D_1(\theta, \phi) = -\frac{4b}{r^4} xy(x^2 - y^2) (\cos \psi \mathbf{e}_\phi - \sin \psi \mathbf{e}_\theta). \quad (23)$$

Substituting Eqn. (21) into Eqn. (23), $D_1(\theta, \phi)$ is written as a function of ζ , ψ , ϕ_i and θ_i . Because the range of ψ is from 0 to 2π , many terms in the integral of D_1 vanish. Denote the integral result as $D_1^e(\theta_i, \phi_i)$ that is dependent of

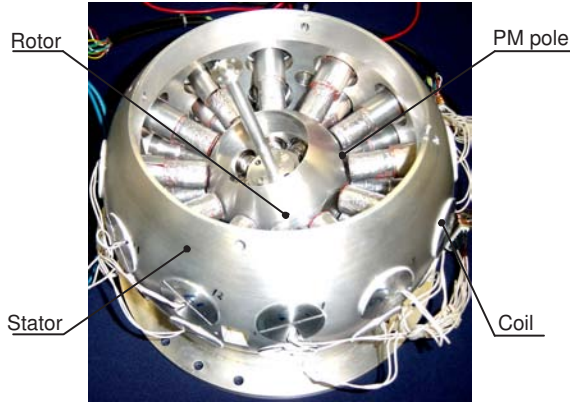


Fig. 7. Prototype of the spherical actuator

the orientation of coils' axes in the rotor frame. We can find the expression of $D_2^e(\theta_i, \phi_i)$ in similar manner. $D_1^e(\theta_i, \phi_i)$ and $D_2^e(\theta_i, \phi_i)$ are defined in Appendix. The unit vectors of \mathbf{e}_ϕ and \mathbf{e}_θ are rewritten in terms of Cartesian coordinates

$$\begin{aligned} \mathbf{e}_\phi &= -\sin \phi_i \mathbf{e}_x + \cos \phi_i \mathbf{e}_y \\ \mathbf{e}_\theta &= \cos \theta_i \cos \phi_i \mathbf{e}_x + \cos \theta_i \sin \phi_i \mathbf{e}_y - \sin \theta_i \mathbf{e}_z. \end{aligned}$$

Substituting them into Eqn. (20) and using $D_1^e(\theta_i, \phi_i)$, $D_2^e(\theta_i, \phi_i)$, we can obtain a 3×1 vector, $\mathbf{f}(\theta_i, \phi_i) = [f_x(\theta_i, \phi_i) \ f_y(\theta_i, \phi_i) \ f_z(\theta_i, \phi_i)]^T$. This vector relates the input current of the i^{th} coil and its output torque by:

$$\mathbf{T}_i = \begin{bmatrix} T_{xi} \\ T_{yi} \\ T_{zi} \end{bmatrix} = T_c \begin{bmatrix} f_x(\theta_i, \phi_i) \\ f_y(\theta_i, \phi_i) \\ f_z(\theta_i, \phi_i) \end{bmatrix} J = T_c \mathbf{f}(\theta_i, \phi_i) J, \quad (24)$$

where $T_c = -M_0 \frac{15}{16\pi} \sqrt{\frac{35}{2}} \frac{cR_r^6}{(5+4\mu_r)} (r_1^{-2} - r_0^{-2})$. Note that $\mathbf{f}(\theta_i, \phi_i)$ is determined by the orientation of the i^{th} stator coil relative to the rotor coordinates. Therefore, the resultant torque of the spherical actuator is orientation-dependant. With n stator coils, we can obtain n torque equations like Eqn. (24). Combining the torque equations for all coils and putting them into a matrix form give

$$\mathbf{T} = T_c \begin{bmatrix} f_x(\theta_1, \phi_1) & f_x(\theta_2, \phi_2) & \cdots & f_x(\theta_n, \phi_n) \\ f_y(\theta_1, \phi_1) & f_y(\theta_2, \phi_2) & \cdots & f_y(\theta_n, \phi_n) \\ f_z(\theta_1, \phi_1) & f_z(\theta_2, \phi_2) & \cdots & f_z(\theta_n, \phi_n) \end{bmatrix} \begin{bmatrix} J_1 \\ J_2 \\ \vdots \\ J_n \end{bmatrix}, \quad (25)$$

where $[J_1 \ J_2 \ \cdots \ J_n]^T$ is a vector of the currents passing through Coil 1, Coil 2, \cdots , Coil n . For brevity, let A be the torque matrix, Eqn. (25) is then $\mathbf{T} = T_c A [J_1 \ J_2 \ \cdots \ J_n]^T$. It can be verified that matrix A is always full rank within the workspace. Therefore, for any orientation of the rotor, input currents can be found to direction the rotor to a neighboring orientation, i.e. there is no singularity within the workspace.

IV. EXPERIMENTAL INVESTIGATION

A. Prototype Development

Based on the working principle discussed in Section I, a research prototype of the spherical actuator has been developed. As shown in Fig. 7, this prototype basically

consists of a ball-like rotor (in the middle) and a shell-like stator. The rotor is connected to the stator through a spherical bearing. It has one layer of eight PM poles which are evenly distributed along its equator. On the other hand, the stator has twenty-four coils which are evenly grouped into two layers and symmetrically placed about its equator.

B. Testbed Setup

A testbed was designed to verify the torque model of the spherical actuator as shown in Fig. 8. The prototype is placed on a platform. The rotor shaft is connected to a 6-DOF force/torque sensor mounted on a 3-axis translational stage. With additional fixtures, this stage can direct the rotor shaft to any specific orientation so that the actuator torque at the corresponding orientation can be measured.

The torque values corresponding to different orientations by varying the separation angle are obtained. Figure 9 illustrates the separation angle. Because the coil axis is in the same plane as the axis of one PM-pole, the torque generated in x - and z - directions are equal to zero. Thus we only need to focus on the torque in y -direction.

C. Experimental Result

Figure 10 shows the curves of experimental and computational results for 0.5A and 1A current inputs respectively. Difference can be found between these curves. It is because that only fundamental term of the scalar potential is used to derive the magnetic field. According to our theoretical model, each component of output torque is directly proportional to the current input. In order to verify this relationship, torque measurements are carried out for different current inputs (0...2 A) by fixing the



Fig. 8. A testbed for force/torque measurement

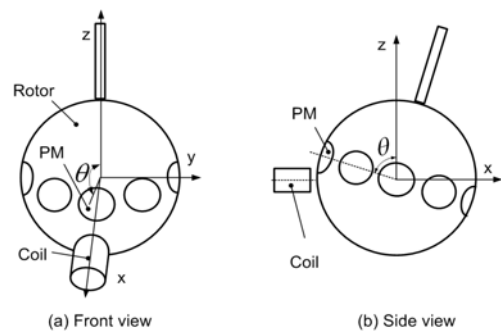


Fig. 9. Separation angle in the force/torque measurement

APPENDIX

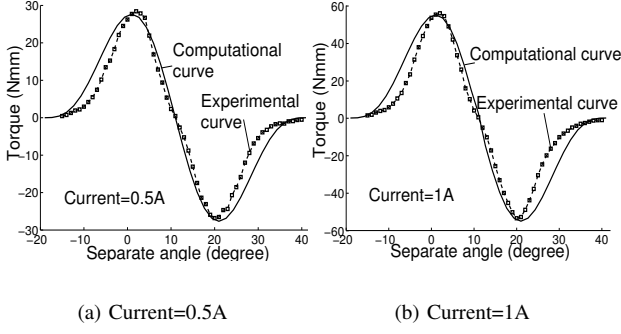


Fig. 10. Comparison of the computational and experimental results

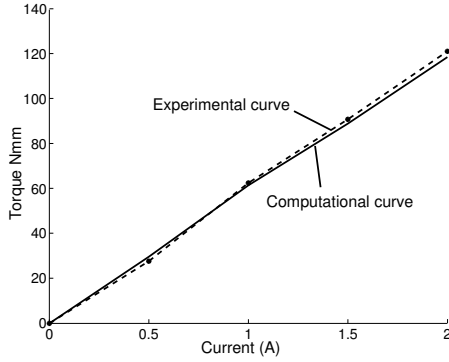


Fig. 11. Linear relation between the current input and the torque output orientation of the rotor. Figure 11 clearly reveals this linear relationship.

V. CONCLUSION

A spherical actuator has been developed to achieve an uniform and continuous 3-DOF rotation in one joint. With knowledge of the pole configuration, Laplace's equation and Poisson's equation of the scalar potential of the PM poles are formulated. By utilizing the boundary conditions and spherical harmonic expansion of the radial component of the magnetization vector, the solution of scalar potentials is obtained. Based on the Lorentz force law, a close-form solution of the torque model of the actuator is achieved. This torque model can be applied to the evaluation and optimal design of the spherical actuator. To verify the theoretical torque model, an experimental testbed was set up to measure the output force/torque of the actuator. Through comparison with experimental results, it proves that the torque model is acceptable. Precision of the model can be improved by having more terms of spherical harmonics in the computation of magnetic field.

ACKNOWLEDGMENT

This work is a collaborative research project among Nanyang Technological University, Singapore Institute of Manufacturing Technology and Georgia Institute of Technology under the project grant U02-A-040B. The authors acknowledge the assistance from Mr. Jialin Su, Dr. Weihai Chen and Mr. Thng Soong Moong Thomas.

$$D_1^e(\theta_i, \phi_i) = 4b\pi \left\{ \begin{bmatrix} -\sin \phi_i & \cos \phi_i & 0 \end{bmatrix}^T \left[\frac{1}{4} \sin^4 \zeta_1 - \frac{1}{4} \sin^4 \zeta_0 \right] \right. \\ \left. (-3 \sin^3 \phi_i \cos \theta_i \sin \theta_i \cos \phi_i + 3 \sin \theta_i \cos^3 \phi_i \cos^3 \theta_i \sin \phi_i + 3 \sin \theta_i \right. \\ \left. \cos \phi_i \cos^3 \theta_i \sin^3 \phi_i + 3 \sin \theta_i \cos^3 \phi_i \cos \theta_i \sin \phi_i) + (-1/4 \cos^4 \zeta_1 \right. \\ \left. + 1/4 \cos^4 \zeta_0) (-4 \cos^3 \phi_i \cos \theta_i \sin \phi_i + 4 \sin^3 \theta_i \cos \phi_i \sin^3 \phi_i \cos \theta_i) \right\} \\ - \left[\cos \theta_i \cos \phi_i \cos \theta_i \sin \phi_i - \sin \theta_i \right]^T \left\{ \left[\frac{1}{4} \sin^4 \zeta_1 - \frac{1}{4} \sin^4 \zeta_0 \right] \left(\frac{9}{2} \right. \right. \\ \left. \left. \sin \theta_i \cos^2 \phi_i \cos^2 \theta_i \sin^2 \phi_i - \frac{3}{4} \sin \theta_i \cos^4 \phi_i \cos^2 \theta_i - \frac{9}{2} \sin \theta_i \right. \right. \\ \left. \left. \cos^2 \phi_i \sin^2 \theta_i + \frac{3}{4} \sin \theta_i \cos^4 \phi_i + \frac{3}{4} \sin^4 \theta_i \sin \theta_i - \frac{3}{4} \sin^4 \theta_i \sin \theta_i \right. \right. \\ \left. \left. \cos^2 \theta_i \right) + (-1/4 \cos^4 \zeta_1 + 1/4 \cos^4 \zeta_0) \left(6 \sin^3 \theta_i \cos^2 \phi_i \sin^2 \phi_i - \sin^3 \theta_i \right. \right. \\ \left. \left. \cos^4 \phi_i - \sin^4 \theta_i \sin^3 \phi_i \right) \right\}$$

$$D_2^e(\theta_i, \phi_i) = a\pi \left\{ \begin{bmatrix} -\sin \phi_i & \cos \phi_i & 0 \end{bmatrix}^T \left[\frac{1}{4} \sin^4 \zeta_1 - \frac{1}{4} \sin^4 \zeta_0 \right] \right. \\ \left. \sin \theta_i \cos^4 \phi_i \cos^3 \theta_i - 18 \sin \theta_i \cos^2 \phi_i \cos \theta_i \sin^2 \phi_i - 3 \sin \theta_i \sin^4 \phi_i \cos^3 \theta_i \right. \\ \left. + 18 \sin \theta_i \cos^2 \phi_i \cos^3 \theta_i \sin^2 \phi_i + 3 \sin \theta_i \cos^4 \phi_i \cos \theta_i + 3 \sin^4 \theta_i \sin \theta_i \right. \\ \left. \cos \theta_i \right) + (-1/4 \cos^4 \zeta_1 + 1/4 \cos^4 \zeta_0) (-4 \sin^3 \theta_i \cos^4 \phi_i \cos \theta_i - 4 \sin^3 \theta_i \right. \\ \left. \sin^4 \phi_i \cos \theta_i + 24 \sin^3 \theta_i \cos^2 \phi_i \sin^2 \phi_i \cos \theta_i) \right\} - \\ \left[\cos \theta_i \cos \phi_i \cos \theta_i \sin \phi_i - \sin \theta_i \right]^T \left\{ \left[\frac{1}{4} \sin^4 \zeta_1 - \frac{1}{4} \sin^4 \zeta_0 \right] \left(12 \sin \theta_i \right. \right. \\ \left. \left. \cos^3 \phi_i \cos^2 \theta_i \sin \phi_i + 12 \sin \theta_i \cos \phi_i \sin^3 \phi_i - 12 \sin \theta_i \sin^3 \phi_i \cos^2 \theta_i \right. \right. \\ \left. \left. \cos \phi_i - 12 \sin \theta_i \sin \phi_i \cos^3 \phi_i \right) + (-1/4 \cos^4 \zeta_1 + 1/4 \cos^4 \zeta_0) \left(16 \sin^3 \theta_i \right. \right. \\ \left. \left. \cos^3 \phi_i \sin \phi_i - 16 \sin^3 \theta_i \sin^3 \phi_i \cos \phi_i \right) \right\}$$

REFERENCES

- [1] Nagasawa H. and Honda S. Development of a spherical motor manipulated by four wires. In *Proceedings of American Society for Precision Engineering*, volume 22, pages 219–221, Scottsdale, Arizona, 2000.
- [2] Toyama S., Sugitani S., and Zhang G. Multi degree of freedom spherical ultrasonic motor. In *Proceedings of 1995 IEEE International Conference on Robotics and Automation*, volume 3, pages 899–904(A), Nagoya, Japan, May 1995.
- [3] Chirikjian G. S. and Stein D. Kinematic design and commutation of a spherical stepper motor. *IEEE/ASME Transactions on Mechatronics*, 4(4):342–353, December 1999.
- [4] Lee K. M., Roth Ronald B., and Zhou Z. Dynamic modeling and control of a ball-joint-like variable-reluctance spherical motor. *ASME Journal of Dynamic Systems, Measurement, and Control*, 118(1):29–40, March 1996.
- [5] Zhou Z. *Real-Time Control and Characterization of a Variable Reluctance Spherical Motor*. PhD thesis, Georgia Institute of Technology, GA, USA, May 1995.
- [6] Wang J., Jewell G. W., and Howe D. Spherical actuators with multiple degrees-of-freedom. In *IEE Colloquium on Limited motion electrical actuation systems*, number 1998/494, pages 8/1–8/6, October 1998.
- [7] Wang J., Jewell G. W., and Howe D. A novel spherical actuator with three degrees-of-freedom. In *IEEE Transactions of Magnetics*, volume 34, pages 2078–2080, June 1998.
- [8] Krause P. C. and Wasynczuk O. *Electromechanical Motion Devices*. McGraw-Hill, Inc., USA, 1989.
- [9] Wang J., Jewell G. W., and Howe D. Modelling of a novel spherical permanent magnet actuator. In *Proceedings of 1997 IEEE International Conference on Robotics and Automation*, volume 145, pages 1190–1195, Albuquerque, New Mexico, April 1997.
- [10] Yan L., Lim C.K., Chen I.M., Yang G.L., Lin W., and Lee K.M. A hybrid approach for magnetic field analysis. In *2004 IEEE Conference on Robotics, Automation and Mechatronics*, pages 530–535, Singapore, December 2004.
- [11] Walter H. *Introduction to the Principles of Electromagnetism*. Addison-Wesley Publishing Company, Inc., USA, 1971.
- [12] Virchenko N. and Fedotova I. *Generalized Associated Legendre Functions and Their Applications*. World Scientific Publication, USA, 2001.